



Spectral Fittings of Warm Coronal Radiation with High Seed Photon Temperature: Apparent Low-temperature and Flat Soft Excess in AGNs

Ze-Yuan Tang^{1,2,3,4,5}, Jun-Jie Feng^{1,2,3,4,5}, and Jun-Hui Fan^{2,3,4,5}

¹ School of Mathematics and Information Science, Guangzhou University, Guangzhou 510006, China; tangzy@mail.ustc.edu.cn and jjfeng@gzhu.edu.cn

² Center for Astrophysics, Guangzhou University, Guangzhou 510006, China

³ Astronomy Science and Technology Research Laboratory of Department of Education of Guangdong Province, Guangzhou 510006, China

⁴ Key Laboratory for Astronomical Observation and Technology of Guangzhou, Guangzhou 510006, China

Received 2024 March 5; revised 2024 May 17; accepted 2024 May 22; published 2024 July 8

Abstract

A warm corona has been widely proposed to explain the soft excess (SE) in X-ray above the 2–10 keV power law extrapolation in Active Galactic Nuclei (AGNs). In actual spectral fittings, the warm coronal seed photon temperature (T_s) is usually assumed to be far away from the soft X-ray, but kT_s can reach close to 0.1 keV in the standard accretion disk model. In this study, we used Monte Carlo simulations to obtain radiation spectra from a slab-like warm corona and fitted the spectra using the spherical-geometry-based routine THCOMP or a thermal component. Our findings reveal that high T_s can influence the fitting results. A moderately high kT_s (around 0.03 keV) can result in an apparent low-temperature and flat SE, while an extremely high kT_s (around 0.07 keV) can even produce an unobserved blackbody-like SE. Our conclusions indicate that, for spectral fittings of the warm coronal radiation (SE in AGNs), kT_s should be treated as a free parameter with an upper limit, and an accurate coronal geometry is necessary when $kT_s > 0.01$ keV.

Key words: galaxies: active – accretion – accretion disks – black hole physics

1. Introduction

In the soft X-ray band (~ 0.3 – 2 keV), an excess (soft excess, SE) above the 2–10 keV power law extrapolation is found in the majority of Active Galactic Nucleus (AGN) spectra (Walter & Fink 1993; Boissay et al. 2016; Liu et al. 2017). There are two prominent explanations for the origin of the SE. One proposed explanation is that the SE is produced by the ionizing reflection of the accretion disk when illuminated by the hot coronal flux (Ross & Fabian 2005; Crummy et al. 2006). However, this ionized reflection model necessitates unusually high black hole spin, compact hot coronae, and sometimes high disk densities to account for relativistic effects and smudge out line emissions (Crummy et al. 2006; Jiang et al. 2018; García et al. 2019; Xu et al. 2021b). Furthermore, numerous observational analyses indicate a weak correlation between the SE and reflection ratio (Mehdipour et al. 2011, 2015; Noda et al. 2013; Matt et al. 2014; Boissay et al. 2016; Porquet et al. 2018; Matzeu et al. 2020; Xu et al. 2021a). As a result, these works preferred an alternative interpretation which consistently provides an excellent fit. According to this interpretation, the SE formation is attributed to the Comptonization of extreme ultraviolet (EUV) disk photons in an optically-thick (with $\tau \sim 10$ – 40) and warm (with $kT \sim 0.1$ – 1 keV) plasma, i.e., “warm corona” (Done et al. 2012; Petrucci et al. 2013). According to studies on variability (De Marco et al. 2013; Kara et al. 2016; Mallick et al. 2021; Zoghbi & Miller 2023) and theory

(Ballantyne 2020; Gronkiewicz et al. 2023), the scale of the warm corona can range from a few to a few tens of gravitational radii (r_g).

In warm coronal spectral fittings, the SE is usually fitted by the Comptonization spectra produced by the routine NTHCOMP (Zdziarski et al. 1996; Życki et al. 1999), or the new version THCOMP (Zdziarski et al. 2020). However, the EUV is very heavily extinguished by the interstellar medium of our Galaxy, and therefore only the high energy part ($\gtrsim 0.3$ keV, i.e., the SE) of the Comptonization spectra is visible. As a result, the spectral fittings can constrain the warm coronal parameters at most, leaving the seed photon temperature (T_s) uncertain.

Although T_s is weakly known, we still need a specific value in spectral fittings. In actual works, the easiest way is to set kT_s much lower than the magnitude of 0.1 keV (e.g., $kT_s = 3$ eV, Petrucci et al. 2018), then the SE profile will be weakly dependent on T_s as photons in the visible part ($\gtrsim 0.3$ keV) have been multiply-scattered and lose their initial information. A very low kT_s is convenient for studying the warm coronal structure, but it would require an unphysically large warm coronal scale to maintain self-consistency (Petrucci et al. 2013, 2018). A more physical idea is that at each radius (r) the $T_s(r)$ follows the local disk temperature $T_d(r)$, which could be close to the magnitude of 0.1 keV (Shakura & Sunyaev 1973; Li et al. 2010; Reynolds 2021). Done et al. (2012) suggested that the disk can be radially divided into two parts: in the outer part, the radiation is semi-blackbody-like, i.e., blackbody radiation ($B_\nu(T)$) with a color temperature correction (f_{col}):

⁵ Authors to whom any correspondence should be addressed.

$I_\nu = B_\nu(f_{\text{col}} T_d)/f_{\text{col}}^4$; in the inner part, the radiation has been Comptonized by the warm and hot coronae, and the $T_s(r)$ is the same as the $T_d(r)$ predicted by the standard accretion disk model (Shakura & Sunyaev 1973). The corresponding public code OPTXAGNF generates the Comptonization component by NTHCOMP, and followed by some other works (e.g., Kubota & Done 2018, 2019; Hagen & Done 2023). However, recently many simulation works suggested that the warm corona should have a vertical structure deep inside (Rózańska et al. 2015; Ballantyne & Xiang 2020; Ballantyne 2020; Petrucci et al. 2020; Gronkiewicz et al. 2023), and therefore an f_{col} should also be considered in the Comptonization region and perhaps the corresponding T_s is underestimated.

Modeling astrophysical Comptonization spectra faces challenges at high seed photon temperatures due to limitations of traditional theories and numerical models. The Kompaneets equation, which underlies codes like NTHCOMP and THCOMP, is strictly valid under two conditions: (1) $h\nu \ll kT_e$ and (2) $kT_e \ll m_e c^2$ (Kompaneets 1957; Sunyaev & Titarchuk 1980). While NTHCOMP/THCOMP have significantly improved the calculation accuracy when $kT_e \sim m_e c^2$ by including the Klein-Nishina scattering cross section, it retains some inaccuracies in calculation when $h\nu$ approaches kT_e (Zdziarski et al. 1996; Życki et al. 1999; Zdziarski et al. 2020, due to the expression of the Klein-Nishina formula, see Equation (1)). The calculation errors will accumulate when T_s approaches T_e , as there are substantial scatterings at $h\nu \sim kT_e$. Furthermore, NTHCOMP/THCOMP adopt a spherical geometry with a sinusoidal seed photon distribution ($\propto (\tau_0/\pi\tau) \sin(\pi\tau/\tau_0)$, where τ_0 is the total radial optical depth) for computational expedience (they followed Sunyaev & Titarchuk 1980), but the actual warm corona is perhaps a slab-like plasma with photons from the bottom (Rózańska et al. 2015; Petrucci et al. 2018; Ballantyne & Xiang 2020; Ballantyne 2020; Petrucci et al. 2020; Gronkiewicz et al. 2023). These differences will further magnify the existing modeling errors. As a result, at high seed photon temperature T_s approaching T_e , the fitted warm coronal temperatures and spectral indices are not reliable.

Several recent studies of slab-like warm coronae have involved (effective) high-temperature seed photons (e.g., Petrucci et al. 2020; Gronkiewicz et al. 2023). However, these studies adopt a vertically temperature-varying plasma which makes defining a representative global temperature difficult. The varying temperature means the final results cannot be straightforwardly estimated, as the final apparent warm coronal temperature depends on the scattering order and can deviate from the optical-depth-weighted average temperature. It is therefore challenging to isolate the influence of high seed photon temperatures on the fitted warm coronal parameters when using a vertically temperature-varying model. Adopting a uniform temperature slab allows the true temperature to be known, which enables us to identify the effects caused by seed photon temperature. In observational analyses, when using

codes like NTHCOMP/THCOMP, the constant warm coronal temperature is already assumed by default (e.g., Jin et al. 2012; Porquet et al. 2018; Matzeu et al. 2020; Xu et al. 2021a; Jin et al. 2022). The fitted temperature then provides a reference for the average warm coronal temperature.

In this study, we utilize the public Monte Carlo simulation code GRMONTY (Dolence et al. 2009) to obtain radiation spectra for the warm coronal region. Subsequently, we fit these spectra using either THCOMP or a thermal component. Then, by assuming a uniform scattering slab in simulations, we have a priori knowledge of the temperature, allowing us to determine the effectiveness of the fitting methods.

The paper is organized as follows: The simulation and fitting methods are introduced in Section 2. In Section 3, we show the numerical results and study how the high seed photon temperature affects the SE profile. In Section 4, we discuss the possible effects on actual spectral fittings. The conclusions are provided in Section 5.

2. Simulation and Fitting Methods

2.1. Simulation Methods

The physical scenario we simulated is straightforward: photons freely traverse within a slab-like electron gas until they undergo scattering; this process is repeated until the photons either escape or are absorbed. Our Monte Carlo simulation kernel for Compton scattering is from the public code GRMONTY (Dolence et al. 2009). The kernel uses the Klein-Nishina differential cross section

$$\frac{2\pi}{\sigma_T} \frac{d\sigma_{\text{KN}}}{d\epsilon'} = \frac{1}{\epsilon^2} \left(\frac{\epsilon}{\epsilon'} + \frac{\epsilon'}{\epsilon} - \sin^2\theta \right), \quad (1)$$

where σ_T is the Thomson cross section, θ is the scattering angle, and ϵ , ϵ' are the initial, final photon energy in the electron rest frame, respectively. It is worth noting that when $\epsilon \sim \epsilon'$, the three terms on the right-hand side of Equation (1) have comparable contributions to the cross section, which makes semi-analytical approximations very difficult, and therefore we need to rely on Monte Carlo simulations.

The configuration of the disk-corona system resembles a slab. The disk occupies a semi-infinite region at the bottom, while the warm corona forms a layer on top. The disk has low temperatures and high densities, and therefore absorption dominates; whereas the warm corona has high temperatures and low densities, and therefore scattering dominates (Done et al. 2012; Petrucci et al. 2018; Ballantyne 2020; Petrucci et al. 2020; Gronkiewicz et al. 2023). Seed photons are emitted isotropically from the disk and undergo scattering processes within the warm coronal region. We assume that the warm corona is a gray atmosphere with pure scattering, and the electrons within are in a thermal distribution. The photons will escape from the system when they cross the upper boundary

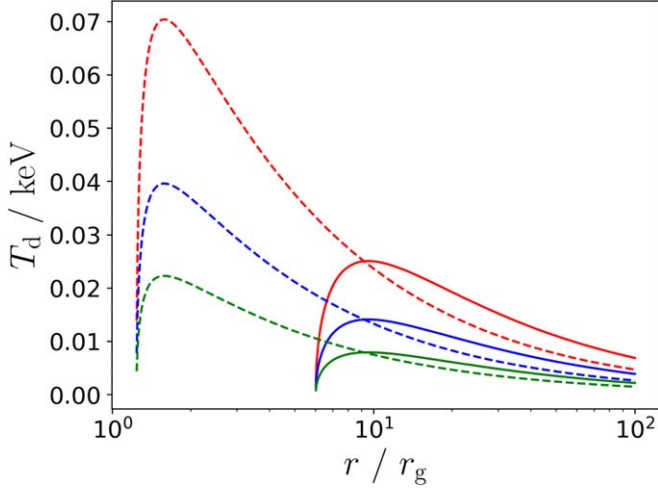


Figure 1. Temperature profiles of relativistic standard accretion disks. The disk temperature T is in unit of keV, and the radius r is in unit of gravitational radius r_g . The black hole mass (M_{BH}) is 10^6 (red), 10^7 (blue) or 10^8 (green), in unit of M_\odot . The black hole spin is 0 (solid) or 0.998 (dashed). The luminosity (L) is 0.3 Eddington luminosity. Readers can scale out the profiles by the relation $T \propto (L/M_{\text{BH}})^{1/4}$.

(the warm coronal surface). Some photons will return to the disk, and most of them will be absorbed but a few of them will be scattered back to the warm corona again. The scattered-back photons can be effectively considered as a special form of emitted photons, and then the overall effect caused by the absorption-scattering competition can be considered as an increase in the seed photon temperature (e.g., Done et al. 2012). In our simulations, a photon will be absorbed immediately after returning to the disk, which means that our setting T_s is indeed an effective temperature.

Now we introduce the method for selecting the input seed photon temperature. Due to the uncertainties in the disk-corona structure, simulation and theoretical works prefer a single temperature as input (e.g., Petrucci et al. 2013; Ballantyne 2020; Petrucci et al. 2020; Gronkiewicz et al. 2023). The final spectrum is a superposition of many spectra with different T_s . Its ultimate characteristics would approach the qualitative properties of the spectrum with a typical T_s within the dominant range. Meanwhile, it is believed that T_s would not significantly deviate from T_d , and therefore the simulation and theoretical works still consider the original T_d as an indication of T_s . The peak temperatures of AGN disks range from 0.01 to 0.1 keV (e.g., Reynolds 2021), while the outer disk temperatures can be as low as a few eVs or even less. To give readers an intuitive impression, a few typical temperature profiles for a relativistic standard accretion disk (Novikov & Thorne 1973) are shown in Figure 1, and readers can also scale out the profiles by the relation $T \propto (L/M_{\text{BH}})^{1/4}$ (where L is the disk luminosity and M_{BH} is the black hole mass). Due to time limitations for simulations, we aim to use as few input values as possible to

obtain spectra that represent the main characteristics across different energy bands and cover the whole energy range. We conducted some preliminary fast simulations to assist with T_s selection. First, for all $kT_s \lesssim 0.01$ keV, the SE ($\gtrsim 0.3$ keV) profile is not affected by T_s , and therefore we set the lowest kT_s in the simulations to 0.01 keV. Second, for $kT_s \gtrsim 0.07$ keV, considerable SE profiles will be blackbody-like, and therefore we set the highest kT_s in the simulations to 0.07 keV. Finally, the current two kT_s values are far apart, and therefore we choose an intermediate value of 0.03 keV, at which the SE profile is affected by T_s but not black-body like. For the three T_s values, 0.01 keV corresponds to a typical peak temperature of ultra-high-mass and low/moderate-accretion-rate AGNs (e.g., early quasars, Wu et al. 2015), or T_d at larger radii of AGNs with higher peak temperature; 0.07 keV corresponds to the peak temperature of low-mass and high-accretion-rate AGNs (e.g., Narrow-line Seyfert 1 (NLS1s) galaxies, Osterbrock & Pogge 1985; Gu et al. 2015); 0.03 keV corresponds to a variety of situations, such as T_d at $\sim 10r_g$ of NLS1s, peak temperature of some luminous quasars (high-mass and high-accretion-rate, e.g., Laurenti et al. 2022), etc.

Our main concern is the warm coronae with low-temperature electrons ($kT_e \in [0.1, 0.4]$ keV). Meanwhile, the warm coronal vertical Thomson optical depth $\tau \in [5, 70]$. Observations and simulations show that these selected value ranges cover most of the corona (see Gronkiewicz et al. 2023, and references therein). The warm coronae outside of these ranges will not affect our results, because they are few in number and their parameter values are always on the same side of the median.

2.2. Fitting Methods

To emulate the actual detectors, the output spectra are divided into frequency channels (I) of logarithmic width $\Delta \log \nu = 0.082$, and the detectors only tell us the photon counts in each channel ($C(I)$). The X-ray detectors cannot receive the distant photons with energies below ~ 0.3 keV because of interstellar absorption. Considering the specific frequencies of the channels in simulations, we set the lower boundary of the fitting band as 0.26 keV, and this value only weakly influences our results as long as the high energy cut-off of SE is visible or not obvious. Meanwhile, in studies of the warm corona, one approach is to analyze the properties of the remaining soft X-ray flux (i.e., SE) after removing the background power-law component. Considering the signal-to-noise ratio, in actual observational works, the upper energy limit of SE is usually set between ~ 1 keV (e.g., Boissay et al. 2016; Zoghbi & Miller 2023) and ~ 2 keV (e.g., Laurenti et al. 2022; Tang et al. 2023), varying in different cases. Therefore, we set the upper boundary of the fitting band as 1.0, 1.2, 2.1 keV in our fittings.

We apply two different methods to fit the output spectra. In the first method we use a thermal component to fit the spectra and get best-fitting blackbody temperatures (T_b). In the second method we utilize the warm corona model. As THCOMP requires, the warm coronal structure is described by warm coronal temperature T_{wc} and photon index Γ (Γ is a function of T_{wc} and τ_{wc}). We further set the input photons in a thermal distribution of T_d . All the seed photons will be Comptonized in the warm coronal rest frame. Then, THCOMP has the capability to generate Comptonization spectra by employing a sinusoidal distribution of seed photons within spherical electron gas. We set $kT_d = 0.01, 0.03, 0.07$ keV in fittings, and since we do not have a priori disk temperature in observational works, T_d does not need to match the seed photon temperature T_s . Following the other warm coronal works (e.g., Waddell et al. 2023), we set $kT_{wc} \in [0.1, 1]$ keV and $\Gamma \in [2.0, 3.5]$.

Following XSPEC (Arnaud 1996), the fit statistic in use for determining the best-fitting model is χ^2

$$\chi^2 = \sum \frac{(C(I) - C_m(I))^2}{(\sigma(I))^2}, \quad (2)$$

where C_m is the model-predicted photon count and $\sigma(I)$ is the simulation error. $\sigma(I)$ is estimated by $\sqrt{C(I)}$ in this work.

We further define a ratio

$$R_{b/c} = \frac{\chi_b^2}{\chi_{wc}^2}, \quad (3)$$

where the subscripts b and wc correspond to the blackbody and warm corona fitting methods, respectively.

3. Numerical Results

3.1. Output Spectra

We first visualize the output spectra and qualitatively analyze the results. Since the photon distribution in a channel is unknown, we approximate the distribution to be uniform and set the energy of the plot point at the geometric mean of the channel boundaries: $E_p = \sqrt{E_{\min}(I)E_{\max}(I)}$.

The output spectra are shown in Figure 2.⁶ There are only three parameters: T_s (decides the low energy cut-off), T_e (decides the high energy cut-off) and τ . In general, when the two energy cut-offs are further from each other (i.e., T_e/T_s is larger), the spectra are more likely similar to the ones produced by THCOMP. For example, in the left-bottom panel ($kT_s = 0.01$, $kT_e = 0.4$), for the spectra corresponding to moderate optical depths (middle curves), they show power-law profiles between their low and high energy cut-offs; while for the spectra corresponding to very small or large optical depths (left or right curves respectively), the power-law profiles are so steep that the energy rollovers are not very obvious, but the power-law

⁶ In this paper, we ignore the symbol k meaning Boltzmann constant in all the figures for simple layout.

kT_e/keV	0.1	0.2	0.3	0.4
τ_r	[30, 65]	[25, 45]	[20, 35]	[20, 30]

Note. The term ‘‘reasonable’’ here means that when the fitting method works well, the best-fitting parameters of the output spectra should be normal in observations.

part can still be distinguished by careful observation. In contrast, none of the spectra in the right-top panel ($kT_s = 0.07$, $kT_e = 0.1$) contains a clear power-law profile, and in fact they look like a thermal bump. It seems that when the two energy cut-offs are close to each other, there will be only a narrow frequency window left to form a power-law component. As a result, when T_e/T_s drops (from bottom-left to top-right panels), the window widths reduce and the spectra are more and more blackbody-like.

In every panel of Figure 2, one can see that the evolution trend of the spectral profile with the optical depth is continuous and monotonic, and the trends are very similar in different panels. As shown, when τ increases, the power-law photon index Γ (if it exists) decreases, and the energies of the two cut-offs increase. Meanwhile, the low energy cut-off increases faster than the high one, which makes all the spectra corresponding to high τ more or less look like a thermal bump. One main difference between the trends should be mentioned here: for high T_e , the scattering is more efficient, and therefore the evolution of the photon index and energy cut-offs will be more dramatic. As a result, the spectra with a small T_e/T_s may not become blackbody-like at a small τ .

3.2. Spectral Fittings

For the warm corona model, the best-fitting spectral parameters of the numerical simulation results are depicted in Figure 3. The fitting results for $\tau = 5$ are not shown here due to too less photon count in the fitting bands. Our simulation range of optical depth is much larger than the reasonable ranges constrained by observations, and therefore almost all the curves of best-fitting parameters more or less trace the fitting boundary. From the $kT_d = 0.01$ keV (solid) fittings in the $kT_s = 0.01$ keV (left column) cases, one can identify the reasonable range, where Γ varies with τ and T_{wc} roughly matches T_e . The reasonable ranges of τ for different T_e are listed in Table 1; notice that these values are just some rough estimates.

In the left column of Figure 3, $kT_s = 0.01$ keV, when kT_d increases from 0.01 (solid) to 0.03 keV (dashed), the fitting parameters are still stable, but when kT_d increases to 0.07 keV (dotted), the best-fitting parameters are counterfactual and oscillating (except the $kT_e = 0.01$ keV case, for which T_{wc} will

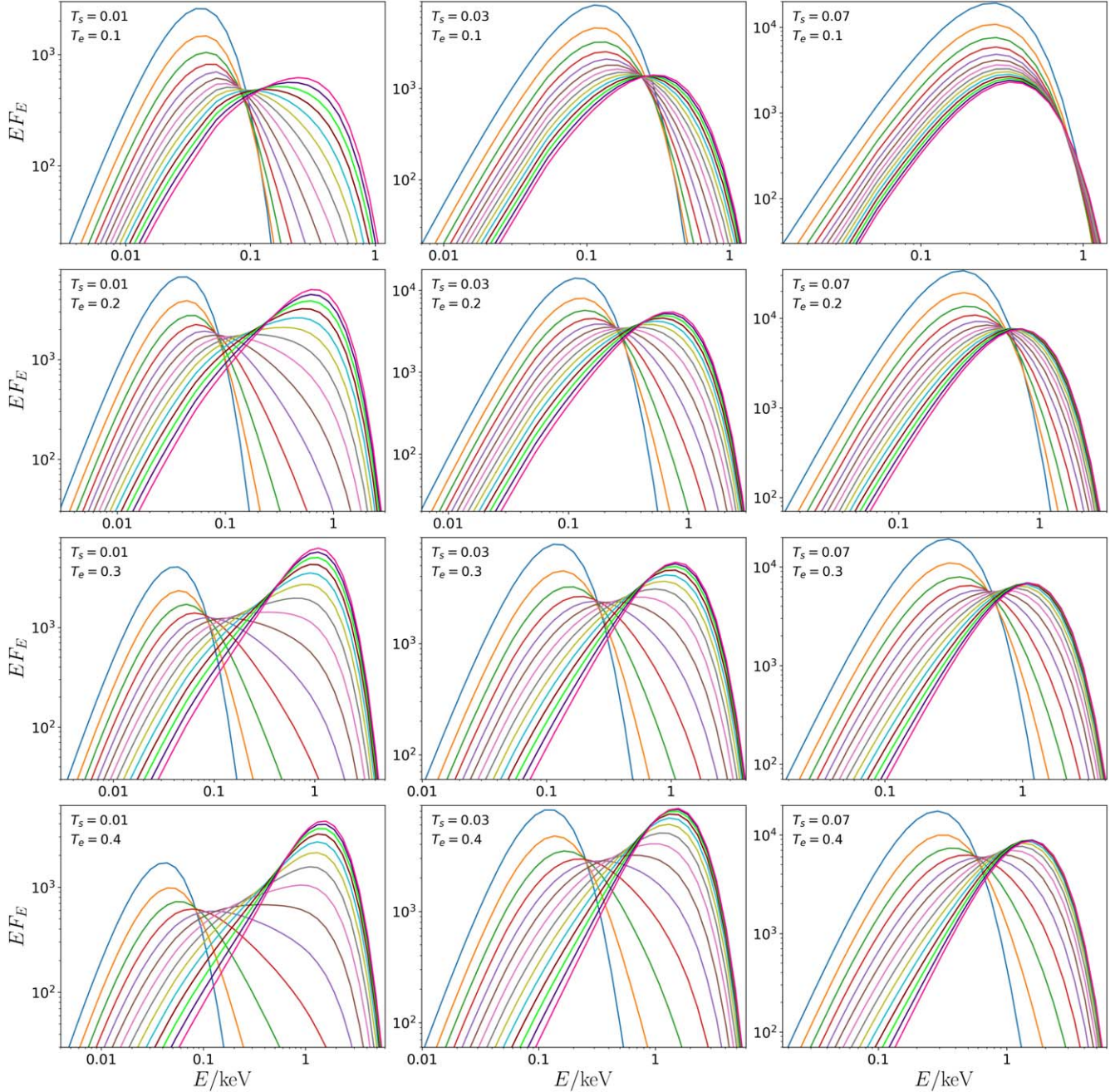


Figure 2. The output spectra of numerical simulations. E of the plot point for a channel is at the geometric mean of the channel boundaries: $E_p = \sqrt{E_{\min}(I)E_{\max}(I)}$. From left to right columns: seed photon temperature $kT_s = 0.01, 0.03, 0.07$ keV. From top to bottom rows: electron temperature $kT_e = 0.1, 0.2, 0.3, 0.4$ keV. In each panel, the curves from left to right correspond to the vertical Thomson optical depth $\tau = 5, 10, 15, \dots, 70$, respectively. From bottom-left to top-right panels, the spectra will transition from THCOMP-like spectra to blackbody-like spectra.

naturally trace the fitting boundary). In the middle column, $kT_s = 0.03$ keV, the overall curve profiles have not changed. However, the T_{wc} of the $kT_d = 0.01, 0.03$ (solid, dashed) fittings in the reasonable ranges are obviously lower than T_e , especially for the $kT_e = 0.3, 0.4$ keV cases. Meanwhile, the Γ

also decreases. In the right column, $kT_s = 0.07$ keV, the best-fitting parameters are quite different. Now the fitting method hardly works when $kT_d = 0.01, 0.03$ (solid, dashed), one phenomenon is that their Γ values are almost 2.0 (lower boundary) everywhere. In addition, for the $kT_d = 0.07$ (dotted) fittings, the parameters seem to be normal, just like the

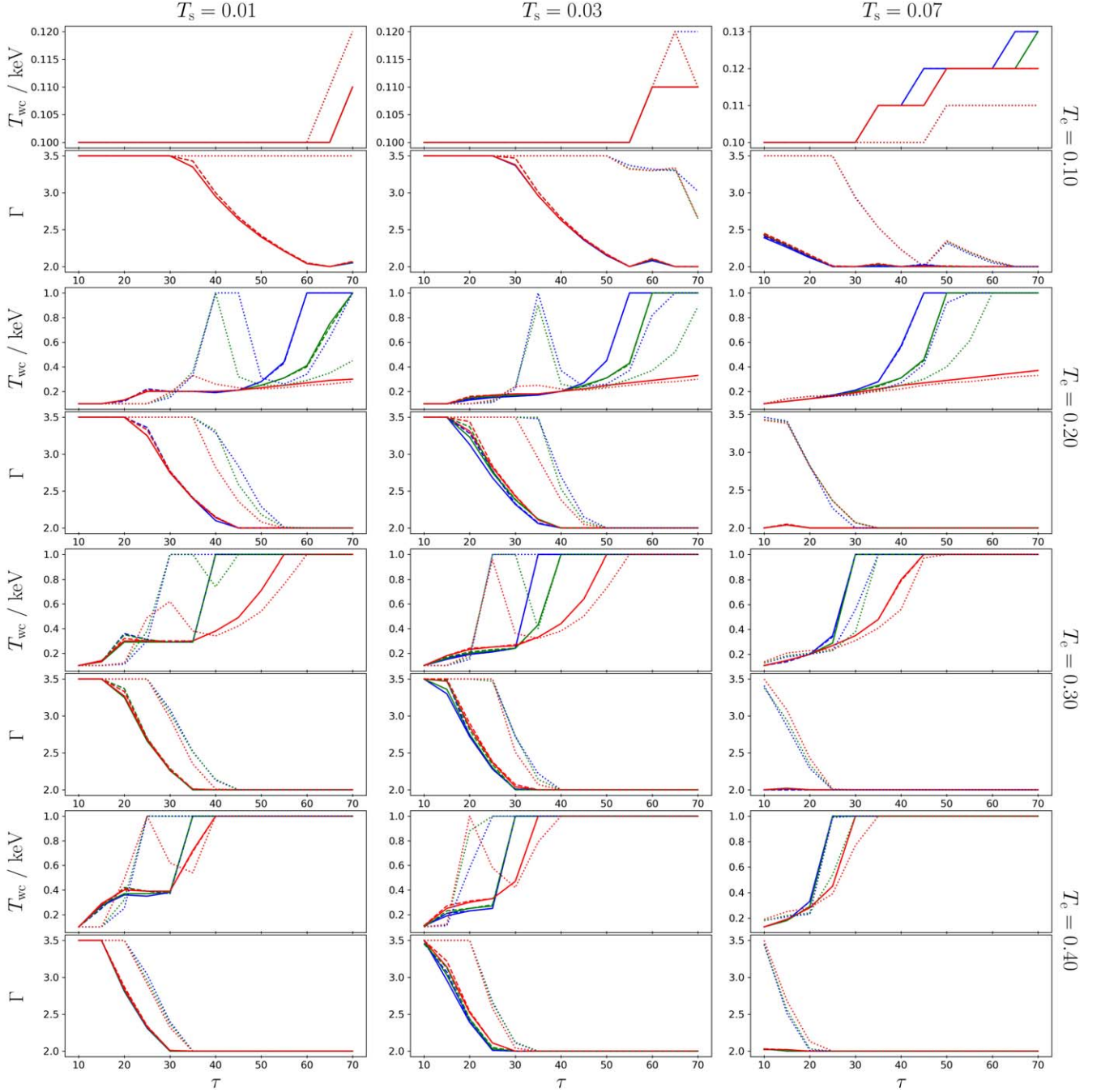


Figure 3. Best-fitting spectral parameters of the numerical simulation results, measured by assuming a warm corona model. τ is the vertical Thomson optical depth. The results of one simulation case are shown in two panels (1×2 , T_{wc} and Γ). The simulation parameters are $kT_s = 0.01, 0.03, 0.07$ keV (from left to right cases), and $kT_c = 0.1, 0.2, 0.3, 0.4$ keV (from top to bottom cases). The fitting disk temperature $kT_d = 0.01$ (solid), 0.03 (dashed), 0.07 (dotted) keV, and the upper boundaries of the fitting band are 1.0 (blue), 1.2 (green), 2.1 (red) keV. Notice that curve number (9) is the same in each panel, though part of the curve is not visible due to high overlap in some panels. In the reasonable range, T_{wc} matches T_c when $kT_s = 0.01$, and decreases with increasing T_s .

$kT_d = 0.03$ (dashed) fittings in the middle column, but indeed the T_{wc} values in the reasonable ranges are also obviously underestimated.

At the end of the discussion for Figure 3, we should mention that the fitting band (in different colors) does not affect the above conclusions: in most of the cases, the differences caused

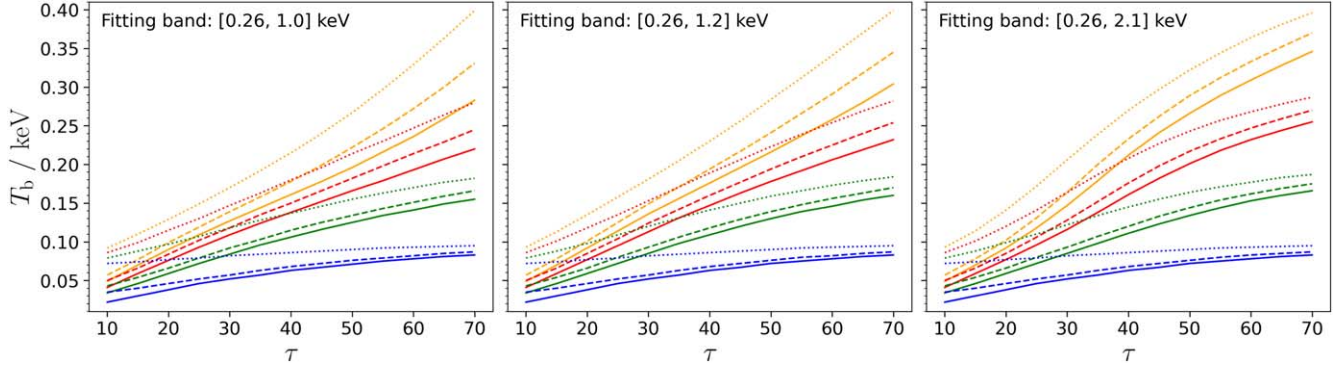


Figure 4. Best-fitting blackbody temperatures (kT_b) of the numerical simulation results. τ is the vertical Thomson optical depth. The simulation parameters are: $kT_s = 0.01$ (solid), 0.03 (dashed), 0.07 (dotted) keV, and $kT_e = 0.1$ (blue), 0.2 (green), 0.3 (red), 0.4 (orange) keV. The fitting bands are listed in the corresponding panels. In general, T_b increases with T_s and T_e , but can hardly exceed the corresponding T_e . The fitting results are insensitive to the fitting band.

by the fitting band are significant only when at least one of the T_{wc} , Γ reaches the fitting boundaries, i.e., when the fitting method works poorly; the only exceptions come from the $kT_d = 0.07$ keV fittings in the $kT_s = 0.01, 0.03$ keV cases, as the red dotted curves show some differences, but in actual fittings T_s will be only underestimated.

For the blackbody model, the best-fitting blackbody temperatures (kT_b) of the numerical simulation results are shown in Figure 4. In general, T_b increases with T_s and T_e , but can hardly exceed the corresponding T_e : for $kT_e \leq 0.2$ keV cases, the upper limitations of T_b seem to be lower than the corresponding T_e ; for $T_e \geq 0.2$ keV cases, anyway T_b does not exceed T_e in simulation ranges. In the reasonable ranges of optical depth, T_b in all the cases can vary from a few tens of eVs to about 0.2 keV. It is worth noting that, unlike the warm corona model, the fitting results of the blackbody model are insensitive to the fitting band.

It is important to test which model fits the results better, and the results are displayed in Figure 5. $R_{b/c} > 1$ indicates that the warm corona model fits better, while $R_{b/c} < 1$ phenomenologically prefers the blackbody model. Here we should mention that the behavior of the warm corona model will be better if we expand the fitting range of Γ , but the unusual parameters may not be very convincible in actual observational works.

As affirmed in Figure 5, when both kT_s and kT_d are ≤ 0.03 keV (solid, dashed curves in the left, middle columns), each fitting curve has a top platform almost overlapping the reasonable range, and $R_{b/c}$ is still larger than 1 when it drops at the edges of the reasonable range. The character suggests that when kT_s is at most moderately high, the warm corona model is at least better within the reasonable range. However, it is clear that the $R_{b/c}$ of the platform decreases with increasing kT_s , and the top platforms move to small τ . As a result, when $kT_s = kT_d = 0.07$ keV (dotted curves in the right column), we find that the blackbody model fits better at large reasonable τ . Moreover, if $kT_d < kT_s = 0.07$ keV (solid, dashed curves in the

right column), the blackbody model will be better in a wide range, especially for the low T_e cases.

4. Discussions

4.1. Decrease of the Best-fitting T_{wc} and Γ

Based on the results shown in Figure 3, it is clear that for electron temperatures (kT_e) greater than 0.01 keV, the THCOMP model fails to fit the spectra well, regardless of whether the seed photon temperature (T_s) is accurately estimated or not. This is evident from the decreasing values of the best-fitting parameters T_{wc} and Γ with increasing T_s . The significant decrease suggests that the effect is primarily due to the seed photon temperature rather than variations in the details of simulations or fittings. Moreover, given the generality of these conclusions (different T_e and T_s), a similar decrease in the fitting parameters can be expected for warm coronae with vertical structures and/or radius-dependent seed photon temperature.

One interesting thing is that the underestimated kT_{wc} cases are around 0.2 keV, which has been suggested as the most common warm coronal temperature (Kubota & Done 2018; Petrucci et al. 2018; Mitchell et al. 2023). Notice that a low temperature warm corona must have a quite large optical depth to produce a flat spectrum (see Figure 3). Therefore, if the underestimation is widespread in observational works, then the required maximum optical depth will decrease. The decrease is favored by simulation works, because a stable Comptonization-dominant region on the disk surface cannot be too thick (conservatively, can hardly reach $\tau = 30$) if it keeps a quasi-uniform temperature (Rózańska et al. 2015; Ballantyne 2020), or the warm corona is thick and thermally unstable (Gronkiewicz et al. 2023); but now the vertical temperature variation is too drastic, and therefore the apparent temperature deviates further from the average temperature, so the radiation spectrum

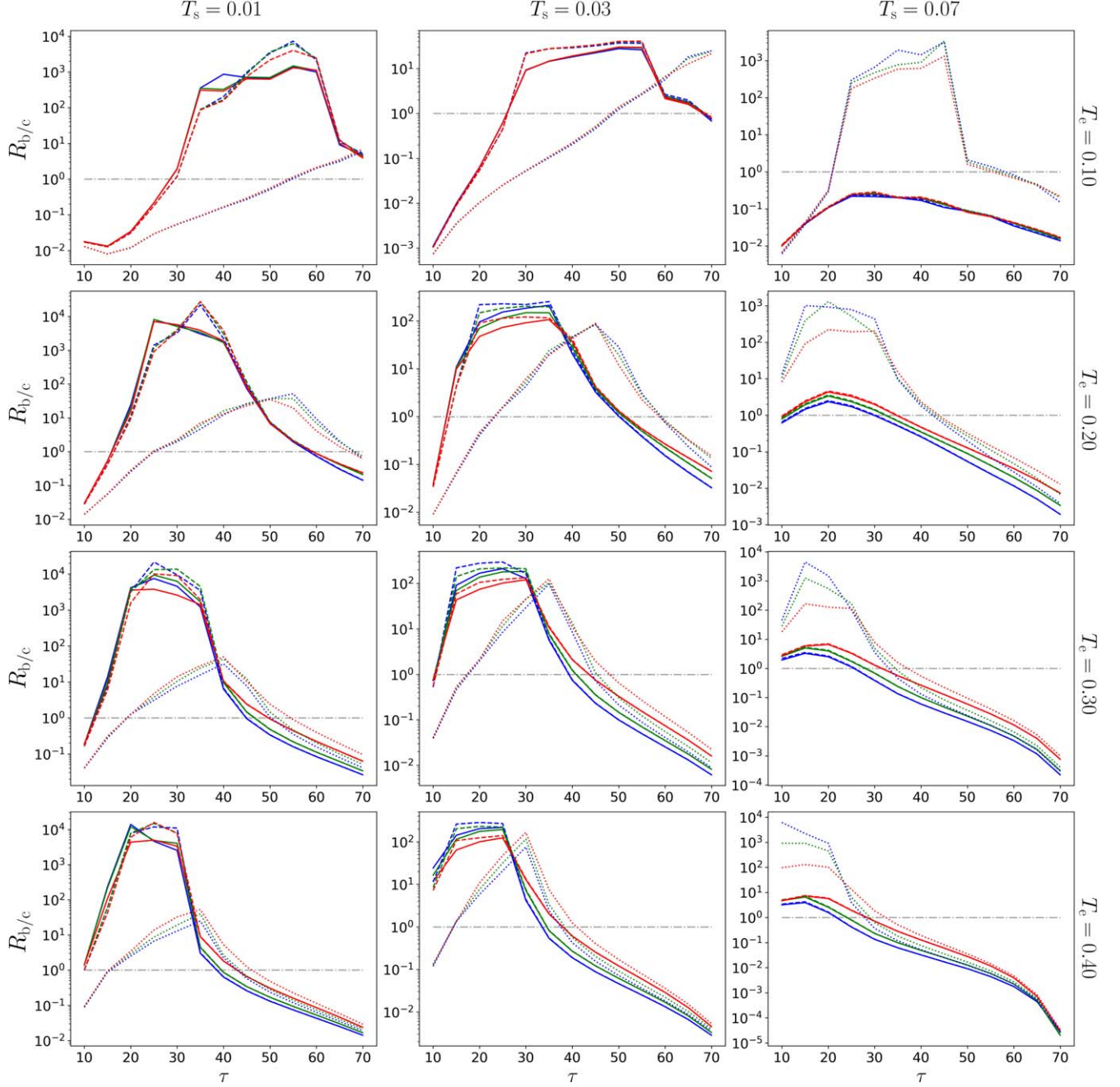


Figure 5. The ratio of χ^2 ($R_{b/c}$) between the warm corona model and blackbody model. $R_{b/c} > 1$ indicates that the warm corona model fits better. τ is the vertical Thomson optical depth. The simulation parameters are $kT_s = 0.01, 0.03, 0.07$ keV (from left to right cases), and $kT_e = 0.1, 0.2, 0.3, 0.4$ keV (from top to bottom cases). The fitting disk temperature $kT_d = 0.01$ (solid), 0.03 (dashed), 0.07 keV, and the upper boundaries of the fitting band are 1.0 (blue), 1.2 (green), 2.1 (red) keV. The horizontal gray dash-dotted lines correspond to $R_{b/c} = 1$. The results indicate that considerable spectra are blackbody-like when $kT_s = 0.07$ keV.

does not match the profile of SE (Tang et al. 2024, in preparation).

A temperature of 0.03 keV is indeed a very common and typical innermost disk temperature for AGNs, but of course not all the disks can touch it. Therefore, the associated phenomena

should have an impact on the fitting results of different samples. We notice that Petrucci et al. (2018) provided fitting results of a sample with simultaneous, high-quality data in both the optical/ultraviolet and X-ray bands observed by XMM-Newton (Mason et al. 2001; Strüder et al. 2001). Their fitting

model assumes that the coronae cover the entire disk, resulting in an inevitable lower fitting temperature for the seed photons. This could potentially underestimate the actual temperature. Their median best-fitting kT_{wc} is 0.24 keV, and the median best-fitting Γ is 2.61 (Appendix C in the original paper). As a comparison, recently Waddell et al. (2023) provided a spectral fitting work for a hard X-ray-selected sample from the eROSITA Final Equatorial Depth Survey (eFEDS) sample (Merloni et al. 2012; Predehl et al. 2021; Sunyaev et al. 2021; Brunner et al. 2022; Liu et al. 2022; Salvato et al. 2022). AGNs in the hard X-ray-selected sample have a high X-ray flux (Nandra et al. 2024). Based on this, we consider AGNs in this sample to have a stronger coronal emission and a weaker disk emission. Consequently, we expect a lower actual T_s and an increase in the best-fitting parameters. For the warm coronal fittings (Table B.5 in the original paper), the median best-fitting kT_{wc} is 0.47 keV, and the median best-fitting Γ is 3.15. Such high values agree with our prediction.

4.2. Blackbody-like SE

From Figure 5, it can be observed that AGNs with extremely high seed photon temperatures (T_s) have the potential to produce blackbody-like SEs. However, whether it is the analysis of individual sources (e.g., Xu et al. 2021a) or statistical work on large samples (e.g., Waddell et al. 2023), there is no evidence to suggest that a blackbody is a better fitting model than the warm corona. Then, since the physical warm corona models suggest that the warm coronal radius decreases with the increasing Eddington luminosity (Kubota & Done 2018, 2019), we further consider NLS1 galaxies, a subclass of AGNs believed to host relatively low-mass supermassive black holes and have high luminosities (Osterbrock & Pogge 1985; Gu et al. 2015). Based on the standard disk model, NLS1s are expected to have relatively higher seed photon temperatures within their compact coronal region, and therefore have blackbody-like or at least flat SEs. However, observations do not agree with this, and the soft photon indices of NLS1s are not flatter than those of Broad-line Seyfert 1 galaxies (Boller et al. 1996; Matzeu et al. 2020; Middei et al. 2020; Yu et al. 2023).

The absence of a blackbody-like SE indicates that the temperature of seed photons may not be able to touch the extremely high temperature allowed by the standard disk model. One possible explanation is that energy is carried away by outflows/winds. For example, NLS1s are known to exhibit strong outflows. Moreover, Cai & Wang (2023) recently reported that the average spectral energy distribution for quasars is much redder than prediction of the standard disk model, suggesting prevalent winds in quasars. Indeed, according to theoretical understanding, it is known that radiation-driven outflows are inevitably generated in high-temperature disks (e.g., Feng et al. 2019). Meanwhile, the relation between

warm coronae and outflows has also been found in simulations (e.g., Rózańska et al. 2015).

Based on the above discussion, we suggest that a physical model should incorporate an upper limit for the seed photon temperature (but the specific value still requires further investigation). This upper limit will modify the distribution of coronal radiation energy between the EUV and soft X-ray bands, and further affect the model-dependent warm coronal radius and intrinsic luminosity of AGNs.

5. Conclusions

In this work, we study how the high seed photon temperature affects the SE in AGNs. We use the Monte Carlo method to simulate the Comptonization process within the warm corona in parameter ranges of $kT_e \in [0.1, 0.4]$ keV, $\tau \in [5, 70]$, and $kT_s = 0.01, 0.03, 0.07$ keV. We then fit the output spectra by THCOMP in parameter ranges of $kT_{\text{wc}} \in [0.1, 1]$ keV, $\Gamma \in [2, 3.5]$, and $kT_d = 0.01, 0.03, 0.07$ keV. We also fit the output spectra by a thermal component. There are two main conclusions:

1. When kT_s is moderately high (0.03 keV in our simulations), the best-fitting T_{wc} and Γ decrease with increasing T_s . The apparent low-temperature and flat SE probably leads to mistaking 0.2 keV as the most common T_e and overestimating the optical thickness of warm coronae. Our results also indicate that low T_s will be more likely to lead to high T_{wc} and steep Γ . This phenomenon can be used to explain why the high X-ray flux AGN sample (Waddell et al. 2023) exhibits higher best-fitting kT_{wc} and Γ compared to the multi-band-selected AGN sample (Petrucci et al. 2018).
2. When kT_s is extremely high, i.e., very close to 0.1 keV (0.07 keV in our simulations), the SE profile will be more likely to be relatively blackbody-like. The absence of a blackbody-like SE in actual AGN spectra indicates that the temperature of seed photons is not able to touch the extremely high temperature allowed by the standard disk model. Therefore, a physical warm corona model should incorporate an upper limit for the seed photon temperature.

Our conclusions indicate that, for spectral fittings of the warm coronal radiation (SE in AGNs), kT_s should be treated as a free parameter with an upper limit, and an accurate coronal geometry is necessary when $kT_s > 0.01$ keV.

Acknowledgments

We thank Mr. Scott Hagen (University of Durham) for advice on the warm corona model. We thank Dr. Jun Li (Guangzhou University) for help on numerical simulation. The work is partially supported by the National Natural Science Foundation of China (NSFC, grant Nos. U2031201 and

11733001) and the Natural Science Foundation of Guangdong Province (2019B030302001). We acknowledge the science research grants from the China Manned Space Project, with No. CMS-CSST-2021-A06. We also acknowledge support from Astrophysics Key Subjects of Guangdong Province and Guangzhou City, and support from Scientific and Technological Cooperation Projects (2020–2023) between the People’s Republic of China and the Republic of Bulgaria, as well as support that was received from Guangzhou University (No. YM2020001).

References

- Arnaud, K. A. 1996, in ASP Conf. Ser. 101, *Astronomical Data Analysis Software and Systems V*, ed. G. H. Jacoby & J. Barnes (San Francisco, CA: ASP), 17
- Ballantyne, D. R. 2020, *MNRAS*, 491, 3553
- Ballantyne, D. R., & Xiang, X. 2020, *MNRAS*, 496, 4255
- Boissay, R., Ricci, C., & Paltani, S. 2016, *A&A*, 588, A70
- Boller, T., Brandt, W. N., & Fink, H. 1996, *A&A*, 305, 53
- Brunner, H., Liu, T., Lamer, G., et al. 2022, *A&A*, 661, A1
- Cai, Z.-Y., & Wang, J.-X. 2023, *NatAs*, 7, 1506
- Crummy, J., Fabian, A. C., Gallo, L., & Ross, R. R. 2006, *MNRAS*, 365, 1067
- De Marco, B., Ponti, G., Cappi, M., et al. 2013, *MNRAS*, 431, 2441
- Dolence, J. C., Gammie, C. F., Mościbrodzka, M., & Leung, P. K. 2009, *ApJS*, 184, 387
- Done, C., Davis, S. W., Jin, C., Blaes, O., & Ward, M. 2012, *MNRAS*, 420, 1848
- Feng, J., Cao, X., Gu, W.-M., & Ma, R.-Y. 2019, *ApJ*, 885, 93
- García, J. A., Kara, E., Walton, D., et al. 2019, *ApJ*, 871, 88
- Gronkiewicz, D., Różańska, A., Petrucci, P.-O., & Belmont, R. 2023, *A&A*, 675, A198
- Gu, M., Chen, Y., Komossa, S., et al. 2015, *ApJS*, 221, 3
- Hagen, S., & Done, C. 2023, *MNRAS*, 525, 3455
- Jiang, J., Parker, M. L., Fabian, A. C., et al. 2018, *MNRAS*, 477, 3711
- Jin, C., Done, C., Ward, M., et al. 2022, *MNRAS*, 512, 5642
- Jin, C., Ward, M., Done, C., & Gelbord, J. 2012, *MNRAS*, 420, 1825
- Kara, E., Alston, W. N., Fabian, A. C., et al. 2016, *MNRAS*, 462, 511
- Kompaneets, A. S. 1957, *JETP*, 4, 730
- Kubota, A., & Done, C. 2018, *MNRAS*, 480, 1247
- Kubota, A., & Done, C. 2019, *MNRAS*, 489, 524
- Laurenti, M., Piconcelli, E., Zappacosta, L., et al. 2022, *A&A*, 657, A57
- Li, G.-X., Yuan, Y.-F., & Cao, X. 2010, *ApJ*, 715, 623
- Liu, T., Buchner, J., Nandra, K., et al. 2022, *A&A*, 661, A5
- Liu, T., Tozzi, P., Wang, J.-X., et al. 2017, *ApJS*, 232, 8
- Mallick, L., Wilkins, D. R., Alston, W. N., et al. 2021, *MNRAS*, 503, 3775
- Mason, K. O., Breeveld, A., Much, R., et al. 2001, *A&A*, 365, L36
- Matt, G., Marinucci, A., Guainazzi, M., et al. 2014, *MNRAS*, 439, 3016
- Matzeu, G. A., Nardini, E., Parker, M. L., et al. 2020, *MNRAS*, 497, 2352
- Mehdipour, M., Branduardi-Raymont, G., Kaastra, J. S., et al. 2011, *A&A*, 534, A39
- Mehdipour, M., Kaastra, J. S., Kriss, G. A., et al. 2015, *A&A*, 575, A22
- Merloni, A., Predehl, P., Becker, W., et al. 2012, arXiv:1209.3114
- Middei, R., Petrucci, P. O., Bianchi, S., et al. 2020, *A&A*, 640, A99
- Mitchell, J. A. J., Done, C., Ward, M. J., et al. 2023, *MNRAS*, 524, 1796
- Nandra, K., Waddell, S. G. H., Liu, T., et al. 2024, The eROSITA Final Equatorial Depth Survey (eFEDS): the hard X-ray selected sample, arXiv:2401.17300
- Noda, H., Makishima, K., Nakazawa, K., et al. 2013, *PASJ*, 65, 4
- Novikov, I. D., & Thorne, K. S. 1973, *Black Holes (Les Astres Occlus)*, Vol. 343 (New York: Gordon and Breach Science Publishers)
- Osterbrock, D. E., & Pogge, R. W. 1985, *ApJ*, 297, 166
- Petrucci, P. O., Gronkiewicz, D., Rozanska, A., et al. 2020, *A&A*, 634, A85
- Petrucci, P. O., Paltani, S., Malzac, J., et al. 2013, *A&A*, 549, A73
- Petrucci, P. O., Ursini, F., De Rosa, A., et al. 2018, *A&A*, 611, A59
- Porquet, D., Reeves, J. N., Matt, G., et al. 2018, *A&A*, 609, A42
- Predehl, P., Andritschke, R., Arefiev, V., et al. 2021, *A&A*, 647, A1
- Reynolds, C. S. 2021, *ARA&A*, 59, 117
- Ross, R. R., & Fabian, A. C. 2005, *MNRAS*, 358, 211
- Różańska, A., Malzac, J., Belmont, R., Czerny, B., & Petrucci, P. O. 2015, *A&A*, 580, A77
- Salvato, M., Wolf, J., Dwelly, T., et al. 2022, *A&A*, 661, A3
- Shakura, N. I., & Sunyaev, R. A. 1973, *A&A*, 500, 33
- Strüder, L., Briel, U., Dennerl, K., et al. 2001, *A&A*, 365, L18
- Sunyaev, R., Arefiev, V., Babyshkin, V., et al. 2021, *A&A*, 656, A132
- Sunyaev, R. A., & Titarchuk, L. G. 1980, *A&A*, 86, 121
- Tang, Z.-Y., Feng, J.-J., & Fan, J.-H. 2023, *MNRAS*, 520, 129
- Waddell, S. G. H., Nandra, K., Buchner, J., et al. 2023, arXiv:2306.00961
- Walter, R., & Fink, H. H. 1993, *A&A*, 274, 105
- Wu, X.-B., Wang, F., Fan, X., et al. 2015, *Natur*, 518, 512
- Xu, X., Ding, N., Gu, Q., Guo, X., & Contini, E. 2021a, *MNRAS*, 507, 3572
- Xu, Y., García, J. A., Walton, D. J., et al. 2021b, *ApJ*, 913, 13
- Yu, Z., Jiang, J., Bambi, C., et al. 2023, *MNRAS*, 522, 5456
- Zdziarski, A. A., Johnson, W. N., & Magdziarz, P. 1996, *MNRAS*, 283, 193
- Zdziarski, A. A., Szanecki, M., Poutanen, J., Gierliński, M., & Biernacki, P. 2020, *MNRAS*, 492, 5234
- Zoghbi, A., & Miller, J. M. 2023, *ApJ*, 957, 69
- Życki, P. T., Done, C., & Smith, D. A. 1999, *MNRAS*, 309, 561